OPEN ACCESS
IOP Publishing
Plasma Physics and Controlled Fusion
Plasma Phys. Control. Fusion **62** (2020) 035005 (8pp)
https://doi.org/10.1088/1361-6587/ab630e

Suppression of electrostatic micro-instabilities in maximum-*J* stellarators

J A Alcusón[1], P Xanthopoulos[1], G G Plunk[1], P Helander[1], F Wilms[2], Y Turkin[1], A von Stechow[1] and O Grulke[1,3]

[1] Max-Planck Institute for Plasma Physics, Wendelsteinstrasse 1, D-17491 Greifswald, Germany
[2] RWTH Aachen University, MathCCES, Schinkelstrasse 2, D-52062 Aachen, Germany
[3] Technical University of Denmark, Anker Engelunds Vej 1, DK-2800 Kgs. Lyngby, Denmark

E-mail: jorge.alcuson@ipp.mpg.de

Received 20 September 2019, revised 26 November 2019
Accepted for publication 17 December 2019
Published 16 January 2020

Abstract

We demonstrate favorable stability properties of maximum-*J* stellarators, exemplified by the Wendelstein 7-X (W7-X) device, in scenarios with low plasma beta. A large number of electrostatic linear gyrokinetic simulations are conducted to scan the relevant parameter space for different configurations, resulting in stability maps that account for the key micro-instabilities thought to drive turbulent transport. These maps exhibit a 'stability valley' in the region where the normalized ion temperature gradient is roughly equal to the normalized density gradient. In this valley, the electrostatic instabilities are partly suppressed thanks to the maximum-*J* property of the W7-X field. This property varies across different W7-X configurations, and this measurable difference is demonstrated to affect the size of the stability valley. Finally, the impact of the isotope effect and collisions on the valley is examined.

Keywords: stellarators, gyrokinetics, plasma instabilities, Wendelstein 7-X, turbulence

(Some figures may appear in colour only in the online journal)

1. Introduction

Energy and particle losses in magnetically confined fusion reactors are attributed to turbulent transport, driven by micro-instabilities, and neoclassical transport (NC), due to collisions. The NC transport, which is minimal in the plasma core of tokamak devices due to their inherent symmetry, is the dominant contribution in stellarators at high enough temperature [1]. The optimisation of the Wendelstein 7-X (W7-X) stellarator has resulted in a NC transport level comparable to that in tokamaks, and at high beta the magnetic configuration tends to become increasingly quasi-isodynamic (QI) [2]. In addition, in certain configurations, W7-X satisfies the maximum-*J* property (for most orbits), which means that the second adiabatic invariant $J = \int m v_{\|} dl$ is a monotonically decreasing function of the plasma radius and thus reaches its maximum value at the magnetic axis [3]. Thanks to these properties, regions of trapped electrons and regions of bad curvature are not coincident, which theoretically should lead to resilience against density-gradient-driven trapped electron modes (TEMs) [4, 5], which are replaced by relatively weak ion-driven TEMs (iTEMs) [6, 7]. Experiments in the first operation campaigns of W7-X show evidence of reduced NC transport [8, 9]. It is therefore expected that the turbulent transport is the main cause of radial losses in discharges where the NC transport is not sufficient to explain the experimental results [10–12], as in the core of tokamak configurations, where the reduced NC contribution leads to a transport dominated by turbulence. The turbulence is generated by micro-instabilities which are driven by gradients of the electron and ion temperatures, and the plasma density [13, 14].

In this study, we assess the effect of the magnetic geometry in W7-X on linear micro-instabilities with gyrokinetic simulations using the GENE code [15] to explore the space of the possible experimental profiles for $T_e/T_i = 1$ (typical in the plasma periphery and the core in high density discharges)

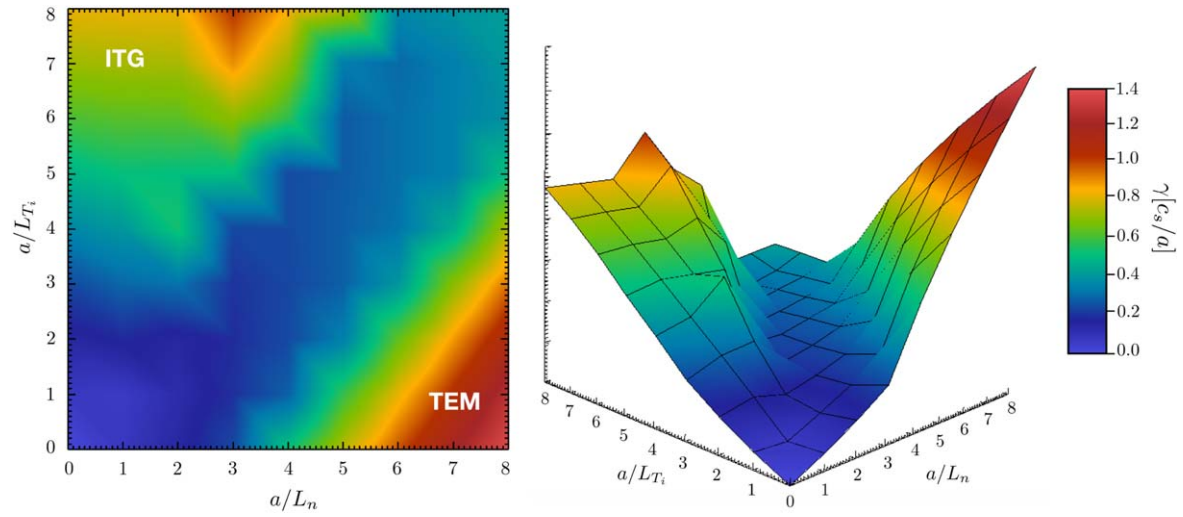

Figure 1. Stability map for W7-X high iota configuration in 2D (left) and 3D (right).

for different magnetic configurations. The central result of this work is that, contrary to tokamaks and non-maximum-J stellarators, W7-X has a wide region in the space of possible profiles—where the transition between the ion temperature gradient (ITG) instability and the trapped electron mode (TEM) occurs—with distinctly reduced linear growth rates, forming a 'stability valley'. W7-X discharges in which hydrogen pellets or laser blow-off injections were performed seem to access this particularly favorable region [16]. Interestingly, the diagnostic analysis of such discharges demonstrate a substantial reduction of the turbulence levels [17]. The aim of the paper is to describe the conditions under which the stability valley is generated, and to study key parameters to control it.

The paper is structured as follows: first, the stability valley is presented and the theoretical background to understand its generation is discussed. The second section deals with magnetic configuration effects in W7-X, whereas the importance of other parameters, such as the normalized electron temperature gradient (ETG), isotope mass, and collisions are studied in the third section. Finally, the main findings are summarized in the last section.

2. Existence of a 'stability valley'

We first present and analyze the electrostatic stability maps associated with various W7-X configurations. These maps are created by plotting the maximum linear growth rate γ from gyrokinetic simulations as a function of the normalized ITG a/L_{T_i} and electron density gradients a/L_{n_e} (here, a is the minor radius of the device and $L_{T_i}^{-1} = -1/T_i\, dT_i/dr$ is the inverse gradient scale length, similarly defined for the density gradient). The electron to ion temperature ration is kept constant at $T_e/T_i = 1$ and their gradients are also taken to be equal. Such maps suggest how to interpret particular experimental conditions with respect to micro-instabilities, hinting at which mechanisms might be involved in the turbulent transport, and allowing different plasmas with similar temperature ratios to be compared. We consider only scales comparable to ion gyroradius but much larger than the electron gyroradius, and thus restrict our attention to ITG and TEM instabilities. We made this choice because, first, these scales are usually where the important contribution to the ion turbulent transport take place in fusion devices. In fact, most of the diagnostics for turbulence in W7-X are designed to measure fluctuations on these scales. Second, we note that in W7-X, radial transport by the ETG instability is theoretically expected to not play an important role compared with the ITGs and TEMs [18]. The latter instabilities are naturally identified through their opposite direction of propagation.

Each map includes 64 linear, local (using the most unstable flux-tube) simulations performed with the GENE code. They have the same parameters; both species are kinetically treated with a resolution of $n_x \times n_y \times n_z \times n_v \times n_w = 31 \times 1 \times 128 \times 48 \times 8$. The stability maps of the study are simulated with the same temperature for ions and electrons $T_i = T_e$ and mainly assume the same electron and ion normalized gradients $a/L_{T_i} = a/L_{T_e}$ and $a/L_{n_i} = a/L_{n_e}$. Compared with [4], we have extended the stability map, using sufficiently large normalized gradients, to capture the complete shape of the valley. By changing the temperature ratio, the shape of the map barely changes; only the overall amplitude is affected. The impact of independently varying a/L_{T_e} is briefly examined in section 4.1.

The stability map in W7-X is characterized by three distinct regions (figure 1): One, on the top-left, where the ITG is the dominant instability with $a/L_{Ti} > a/L_{ne}$; second, on the bottom-right, dominated by TEM, propagating in the electron diamagnetic drift direction, with $a/L_{n_e} > a/L_{T_i}$; and finally, a third region along the main diagonal, around $\eta_i = L_{n_e}/L_{T_i} \approx 1$, where the linear growth rate is significantly reduced or close to zero. In this region of the map, the plasma can either have a dominant mixed ITG/TEM mode or two separated, reduced ITG and TEM modes propagating in the ion direction.

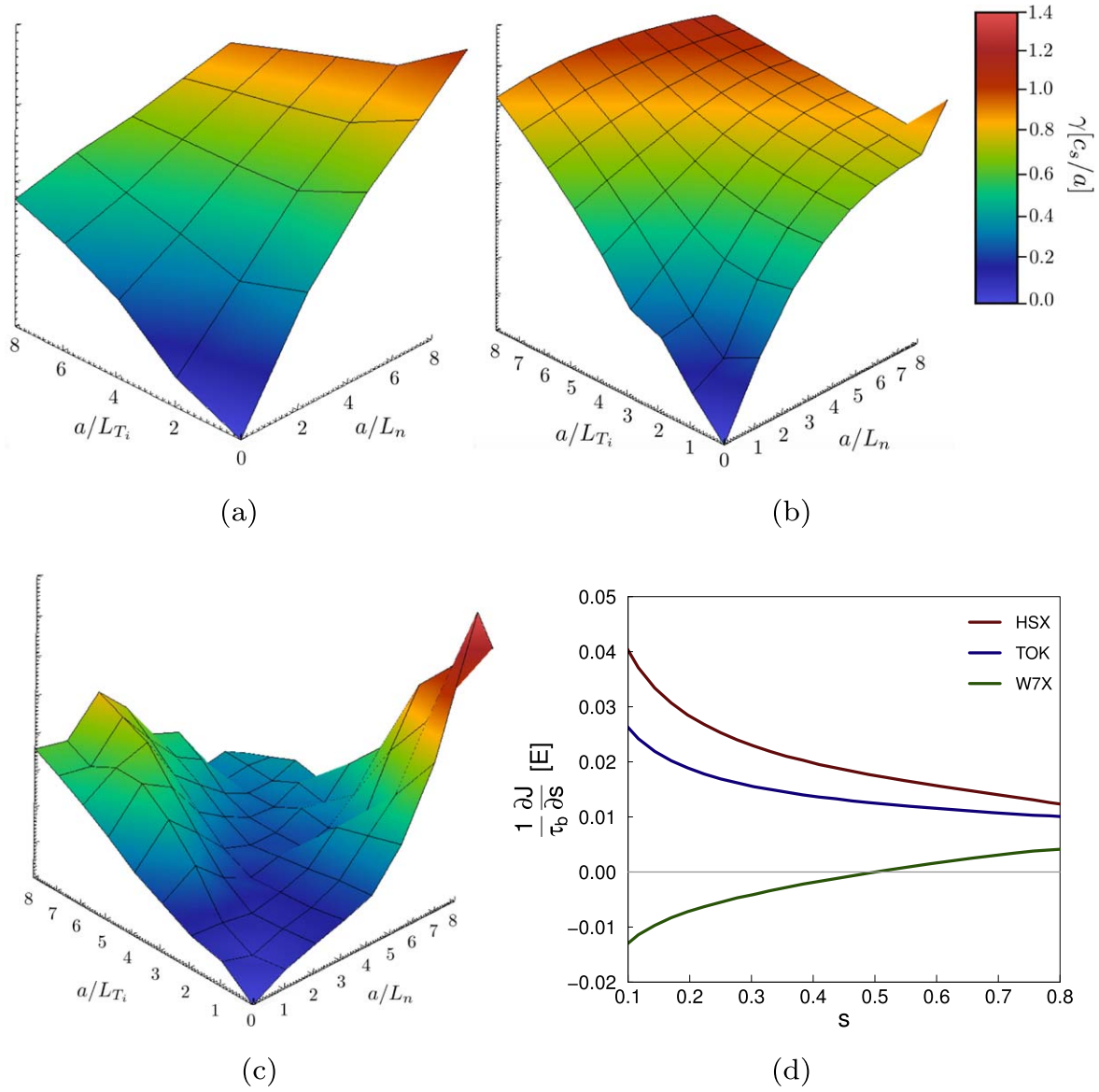

Figure 2. 3D stability maps for Deuterium plasmas in some magnetic configurations: (a) tokamak (b) HSX (c) W7-X at $s = r^2/a^2 = 0.25$. (d) Maximum-J property along the radial direction for these configurations.

2.1. Maximum-J criterion

The valley of reduced growth rate, exhibited by the stability map, is produced by the peculiar geometry of Wendelstein 7-X, in particular its maximum-J property. The stability maps for a typical tokamak, a non-maximum-J stellarator (HSX) and W7-X are compared in figure 2. In the first two cases, the map shows a monotonic increase of the linear growth rate with higher gradients, in contrast to W7-X, with its characteristic stability valley along the main diagonal $\eta_i \approx 1$. This last result demonstrates a failing of the naive intuition connecting stronger free energy sources (gradients) with higher linear growth rates. At the same time, figure 2(d) shows the variation of $\frac{1}{\tau_b}\frac{\partial J}{\partial s}$ along the radial direction for these three configurations, where τ_b is the averaged bounce time for deeply trapped particles, at the location where the curvature is most unfavorable, and $s = r^2/a^2$. The tokamak and HSX configurations have $\frac{1}{\tau_b}\frac{\partial J}{\partial s} > 0$, which means that they are minimum-J configurations (J is a monotonically increasing function with a minimum on the axis), whereas W7-X has $\frac{1}{\tau_b}\frac{\partial J}{\partial s} < 0$, the so-called maximum-$J$ property.

In tokamaks, the ITG instability is mitigated as the density gradient is increased, if electrons are assumed adiabatic. Once, however, kinetic electrons are included, the density gradient increases the linear growth rate γ, signaling the transition to a dominant TEM instability [14]. In configurations like W7-X, however, this situation is entirely different, since the ITG enjoys a gradual reduction as the density gradient becomes stronger, due to the influence of trapped electrons. In addition, the TEM activity is suppressed for specific parameters [4, 5], or can persist in a weakened form when driven by ions (iTEM) [6, 7]. The reduction of the ITG together with the weaker TEM activity, typically co-existing as a 'mixed mode', produce a transition region where the maximum growth rate is substantially reduced, thanks to the

stabilizing effect of the density gradient. These processes are explained mathematically below. In the theory of iTEMs [7], we have a quadratic dispersion relation

$$P\omega^2 + Q\omega + R = 0, \tag{1}$$

$$\omega = -\frac{Q \pm \sqrt{Q^2 - 4PR}}{2P} = \mathbb{R}[\omega] + i\gamma, \tag{2}$$

where the real part of the frequency and the growth rate are defined as

$$\mathbb{R}[\omega] = -Q/2P, \tag{3}$$

$$i\gamma = \frac{i\sqrt{4PR - Q^2}}{2P} \tag{4}$$

with P, Q and R defined as

$$P = \int_{-\infty}^{+\infty} \left[1 + \frac{T_e}{T_i}(1 - \Gamma_0)\right] |\phi|^2 \frac{dl}{B} - \frac{1}{2}\int_{1/B_{max}}^{1/B_{min}} \sum_j \tau_j |\overline{\phi}_j|^2 d\lambda, \tag{5}$$

$$Q = \frac{\omega_{*i} T_e}{T_i} \int_{-\infty}^{+\infty} [\Gamma_0 - \eta_i b(\Gamma_0 - \Gamma_1)] |\phi|^2 \frac{dl}{B} + \frac{\omega_{*e}}{2} \int_{1/B_{max}}^{1/B_{min}} \sum_j \tau_j |\overline{\phi}_j|^2 d\lambda, \tag{6}$$

$$R = \frac{\omega_{*i} T_e}{T_i} \int_{-\infty}^{+\infty} \hat{\omega}_{di} \left[\Gamma_0 - \frac{b(\Gamma_0 - \Gamma_1)}{2} + \eta_i \Gamma_0 (1 - b)^2 + \eta_i b \left(\frac{3}{2} - b\right)\Gamma_1\right] |\phi|^2 \frac{dl}{B} + \frac{3(1 + \eta_e)\omega_{*e}}{4} \int_{1/B_{max}}^{1/B_{min}} \sum_j \widetilde{\omega}_{dej} \tau_j |\overline{\phi}_j|^2 d\lambda = R_i + R_e, \tag{7}$$

where l is the arc-length along the magnetic field, l_0, l_1 its value at two consecutive bounce points, $\lambda = v_\perp^2/(v^2 B)$ and $b = k_\perp^2 m_i T_i/(eB)^2$. The symbol

$$\tau_j = \int_{l_1}^{l_2} \frac{dl}{\sqrt{1 - \lambda B(l)}}$$

is proportional to the time between two consecutive bounce points and $\overline{\phi}$ the bounce-averaged electrostatic potential between these points. Furthermore, ω_{*i} is the diamagnetic frequency, ω_{di} the ion drift frequency, $\bar{\omega}_{de}$ is the orbit-averaged electron drift frequency and $\Gamma_n(b) = I_n(b)e^{-b}$ with I_n the nth-order modified Bessel function. The first term in equation (7), the ion contribution to the instability, is denoted as R_i and the remaining term, the electron contribution, is denoted as R_e. P is positive definite [7], which means that in order to have an instability $R > 0$ is necessary (equation (4)). In general both terms in R can be positive and contribute to destabilization, and we know from [3] that

$$\omega_{*e}\bar{\omega}_{de} = -\frac{k_\alpha^2 T_e}{e^2\tau}\frac{d\ln n_e}{ds}\left(\frac{\partial J}{\partial s} - \frac{k_s}{k_\alpha}\frac{\partial J}{\partial \alpha}\right). \tag{8}$$

In omnigenous (which also includes quasi-isodynamic) configurations $\frac{\partial J}{\partial \alpha} = 0$. Alternatively, if $k_s = 0$ (the ballooning angle is set to 0), this expression reduces to

$$\omega_{*e}\bar{\omega}_{de} = -\frac{k_\alpha^2 T_e}{e^2\tau}\frac{d\ln n_e}{ds}\frac{\partial J}{\partial s}. \tag{9}$$

Assuming typical profiles, with $\frac{dn_e}{ds} < 0$, the inclusion of the maximum-J condition $\frac{\partial J}{\partial s} < 0$ in the last expression will make $R_e < 0$, and electrons help to stabilize the mode [7]. On the other hand, the typical sign for the ion contribution in the unfavorable curvature region $\omega_{*i}\hat{\omega}_{di} > 0$ will produce $R_i > 0$ and ions will drive the instability. This means that if we can find situations where the electron and ion contributions are similar ($R_e \sim -R_i$), then the instability is entirely suppressed or significantly reduced. The contributions from both species each have two terms, one associated with the density gradient and another one associated with the temperature gradient. With the appropriate balance between these terms, the electron contribution outweighs the ion contribution and the instability can be suppressed, creating the valley. Note that the ion and electron density gradients are equal (quasi-neutrality) and our study mainly considers equal temperatures. Thus for clarity, a representation of equation (7) grouping the terms proportional to the temperature gradient (terms with $\eta_{i,e}$) in $R_{\nabla T}$, and the rest of the terms, proportional to the density gradient, in $R_{\nabla n}$ is useful. In this representation both terms can be positive or negative.

Hollow density profiles ($dn_e/ds > 0$) are in principle possible but have never been encountered in W7-X discharges thus far. For such profiles, $R_e > 0$ for a maximum-J device, and consequently the stabilizing effect of the electrons is reversed and the stability valley disappears, as it is indeed confirmed by our simulations.

3. Configuration effects on the valley structure

The degree to which the maximum-J property is satisfied varies between different magnetic configurations of W7-X (which are realised by varying the currents on the 70 superconducting coils), and so does therefore the valley structure. As shown in figure 3, all the W7-X configurations considered demonstrate a valley, except for the low mirror configuration, figure 3(d). The main differences among W7-X configurations are the width and depth of the stability valley. Both high mirror and high iota configurations have a deep valley, where the strong reduction of the instability leads to low linear growth rates (blue region), with the valley for the high mirror configuration being the widest. This is due to the property of the high mirror configuration displacing trapped electrons away from regions of unfavorable curvature. Actually, this effect is enhanced for W7-X configurations with even higher mirror ratio, although above a specific level of this ratio no significant improvement regarding the maximum-J property is found. On the other hand, the standard configuration shows a shallow valley, where the linear growth rate is reduced but not as much as in the other two cases (light-blue and green regions).

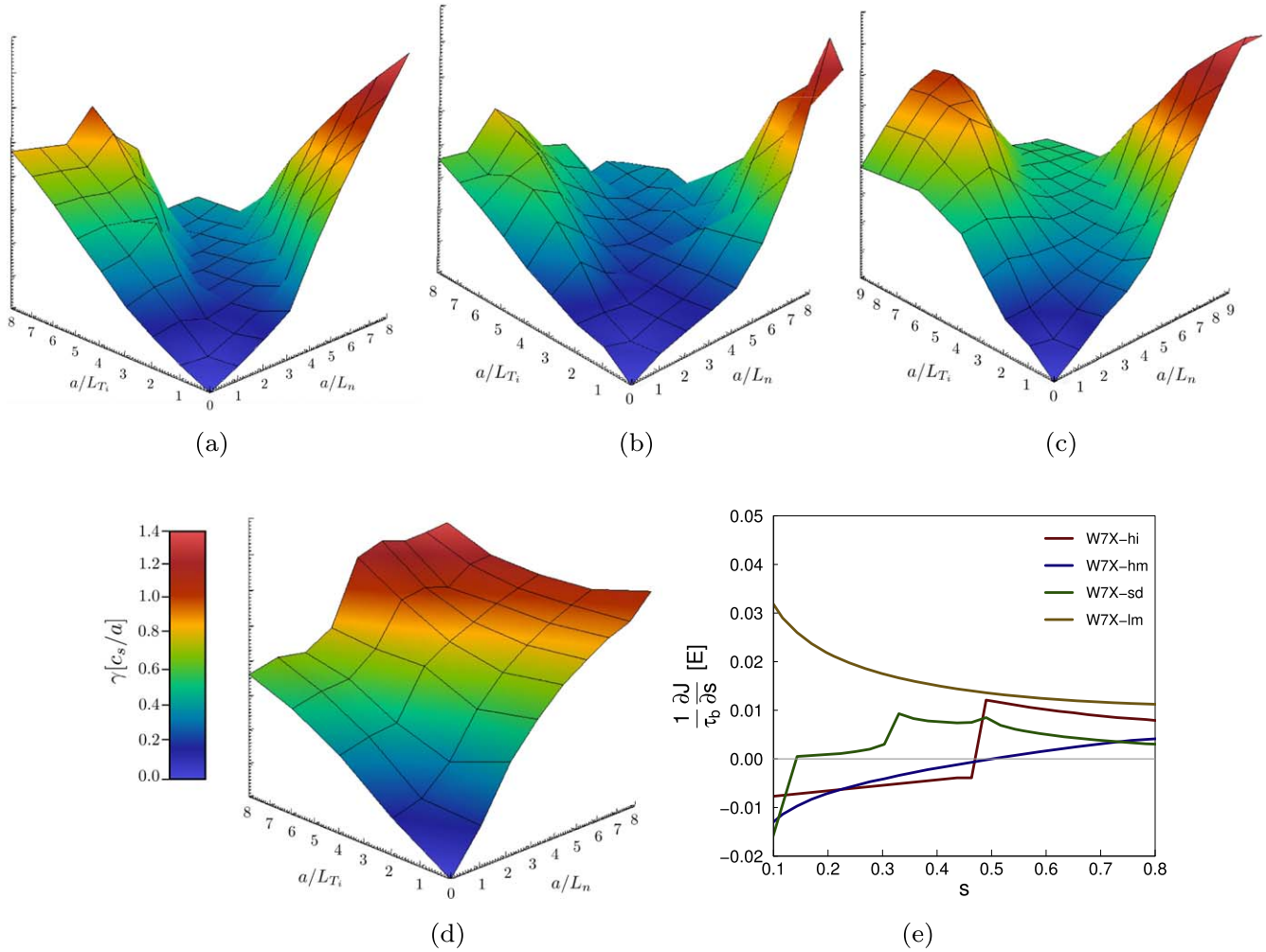

Figure 3. 3D stability maps for Deuterium plasmas in (a) high iota (b) high mirror (c) standard and (d) low mirror W7-X configurations at $s = 0.25$. (e) Figure of merit for the maximum-J property along the radial direction for the high iota (hi), high mirror (hm), standard (sd) and low mirror (lm) configurations.

These findings can be readily connected to a specific measure for the description of the maximum-J property. The quantity $\frac{1}{\tau_b}\frac{\partial J}{\partial s}$ is different in each configuration, leading to variation in the size of the stabilizing term, R_e in equation (7). The radial dependence of this measure for each W7-X configuration is plotted in figure 3(e). The configurations with more negative values of $\frac{1}{\tau_b}\frac{\partial J}{\partial s}$ indeed do show deeper valleys with stronger suppression of the growth rate (stability maps are generated at $s = 0.25$). Furthermore, the low mirror configuration is the only one far from the maximum-J property with $\frac{1}{\tau_b}\frac{\partial J}{\partial s} > 0$, which suggests absence of a valley in the stability map, figure 3(d), similar to what is observed in the tokamak or other non-maximum-J stellarators. This result is especially noteworthy for W7-X, because it enables a comparison of the possible effects of the valley using the low mirror configuration as a counter-example in the same device. The standard configuration, for the magnetic surface considered, is close to constant-J ($\frac{1}{\tau_b}\frac{\partial J}{\partial s} \approx 0$) producing a shallow valley. This means that stabilization is observed, but the effect is weaker than in the high mirror or high iota configurations, where the growth rates are close to zero.

In order to characterize the width of the valley, we can define the direction perpendicular to the $\eta = 1$ diagonal. Along that direction, the valley can be expanded towards $a/L_T > a/L_n$ (up-left in the map) suppressing the ITG instability, or towards $a/L_T < a/L_n$ (down-right in the map) suppressing the TEM instability. For instance, in the high mirror configuration, where the valley is wider than in other configurations due to a greater suppression of the ITG mode.

4. Controlling the stability valley

Apart from the magnetic configuration, there are certain plasma parameters that can be used to modify the valley. Some of them are present in equation (7), like the normalized ETG a/L_{T_e} (included in terms with η_e) and the isotope effect (embedded in the parameter b). Other effects, like collisions, require the inclusion of more terms in the iTEM model.

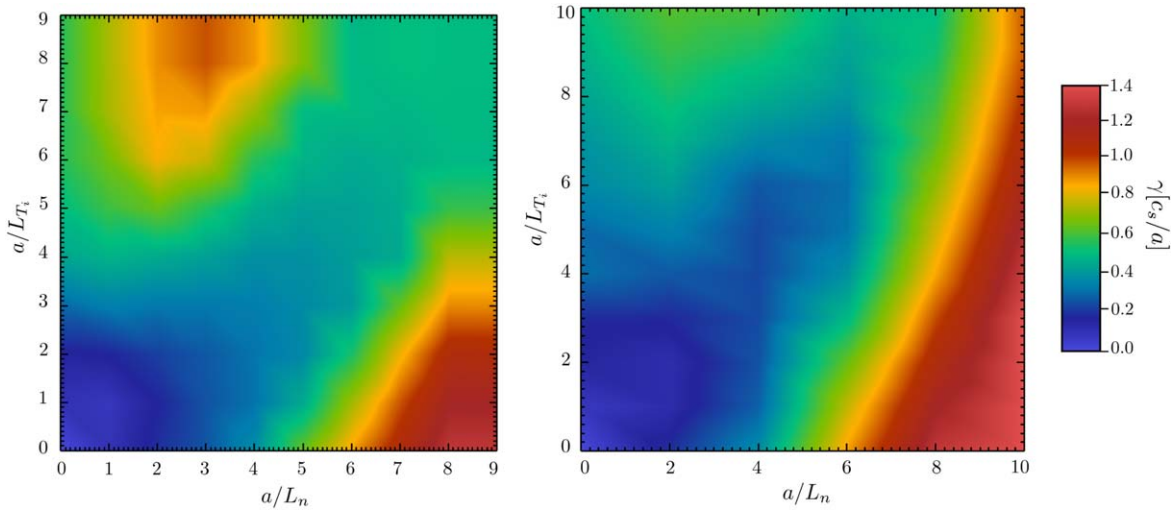

Figure 4. 2D stability maps for W7-X standard configuration with $a/L_{T_e} = a/L_{T_i}$ (left) and $a/L_{T_e} = 0$ (right) and Deuterium plasmas.

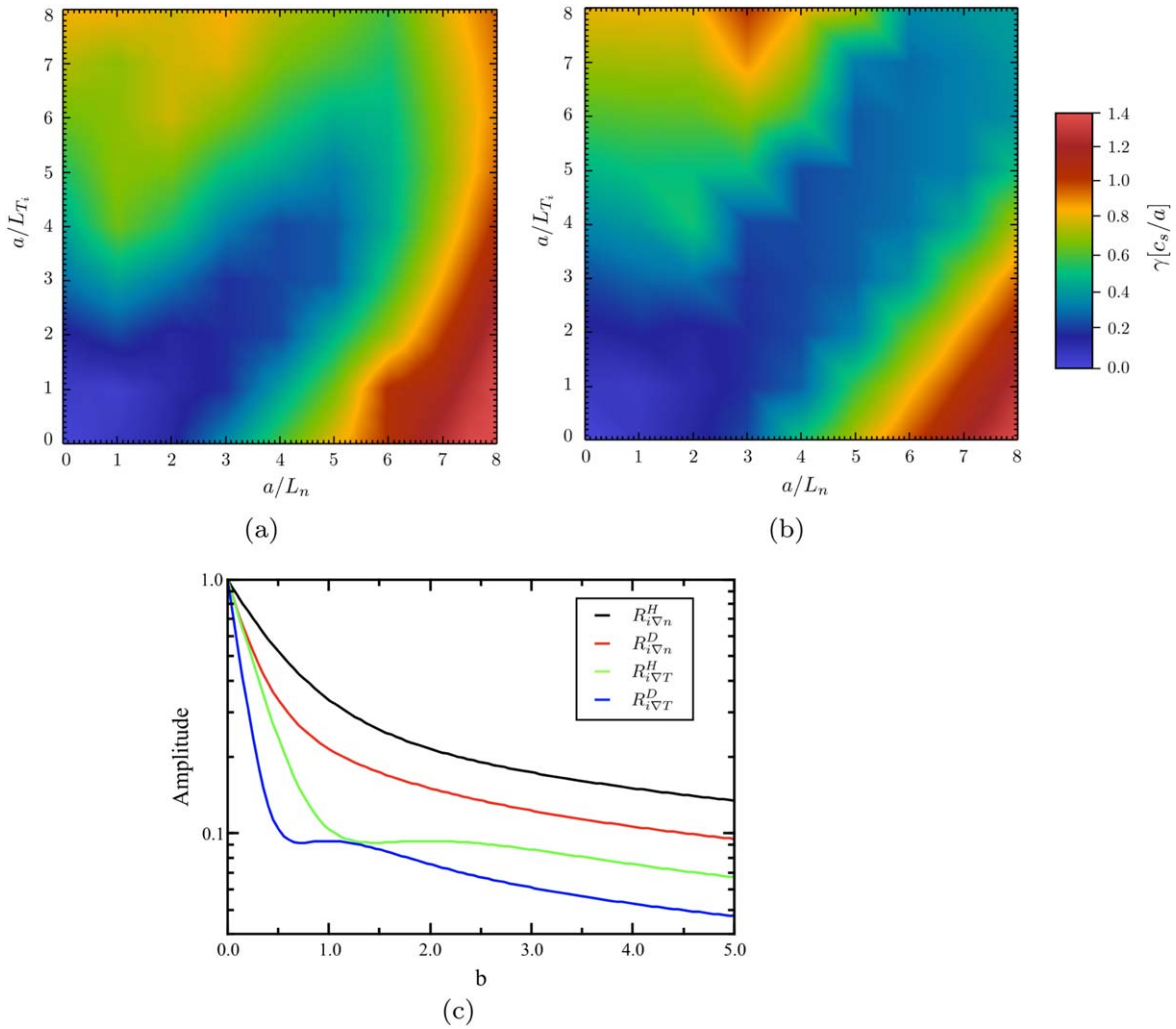

Figure 5. 2D stability maps for W7-X high iota configuration with (a) Hydrogen and (b) Deuterium. (c) $R_{i\nabla n}$ and $R_{i\nabla T}$ weight terms of the iTEM instability considering Hydrogen (H) and Deuterium(D).

4.1. Effect of the ETG

The impact of a/L_{T_e} is studied comparing a map with $a/L_{T_e} = 0$ with the previous analyzed condition where $a/L_{T_e} = a/L_{T_i}$, as in figure 4 for the standard configuration of W7-X. In general, a/L_{T_e} stabilizes somewhat the TEM instability (right-side of the map, $a/L_n \approx 8$), due to the further decrease of $R_e < 0$ in equation (7) through η_e. At the same time, a/L_{T_e} destabilizes a mode for intermediate density gradients and high temperature gradients (top-center region of the maps, $a/L_n \approx 3$ and $a/L_T \approx 8$) in figure 4. This mode is a mixed ITG-iTEM mode where the iTEM instability seems to be temperature driven. The net result from both effects is that the valley is pushed down to slightly smaller η_i values, becoming more shallow as a/L_{T_e} is increased.

4.2. Isotope effect

The isotope mass is also an important parameter in the iTEM model. Comparing the stability maps for the W7-X high iota configuration with Hydrogen and Deuterium, figure 5, a significant difference can be observed for larger normalized gradients (top-right corner of the maps). In the case of Deuterium, the valley is extended along the diagonal $\eta \approx 1$, for Hydrogen the valley ends at lower normalized gradients. This means that W7-X Deuterium plasmas are more stable than Hydrogen ones, and thus we expect more favorable regions on the map for Deuterium discharges.

We can use the iTEM model for a qualitative analysis of the isotope effect. In equation (7), the electron contribution, R_e, is unaltered as it does not depend on the ion mass. As for the first term in equation (7), the ion contribution, the isotope mass is included in the parameter $b = k_\perp^2 m_i T_i/(eB)^2$. Grouping the ion terms in two, one associated to the temperature gradients (proportional to η_i) and one associated to the density gradients, we have

$$R_i = \int (R_{i\nabla n}\omega_{*i}\hat{\omega}_{di} + R_{i\nabla T}\omega_{*i}\eta_i)|\phi|^2 \frac{dl}{B}, \tag{10}$$

$$R_{i\nabla n} = \Gamma_0(b) - \frac{b(\Gamma_0(b) - \Gamma_1(b))}{2}, \tag{11}$$

$$R_{i\nabla T} = \Gamma_0(b)(1 - b)^2 + b(3/2 - b)\Gamma_1(b). \tag{12}$$

The weights for the density and temperature effects equations (11)–(12) are monotonically decreasing functions of b, which it is itself proportional to ion mass, as we observe in figure 5(c). When the latter parameter is increased, the stability valley is thus extended by suppression of the TEM instability. The isotope effect is visible only when both normalized density and temperature gradients are high. In this case, the ion contribution R_i, can be reduced due to the isotope mass, down to the level set by the stabilizing electron contribution (which is unaffected). Both contributions are proportional to the gradients but only one is reduced by the isotope effect which suggest that the reduction of R_i is amplified with high gradients when it is compared with R_e. Also, the iTEM mode could be more strongly influenced by isotope in the 'fluid' limit, approached at large gradients ($\omega_{*i} \gg \omega_{di}$).

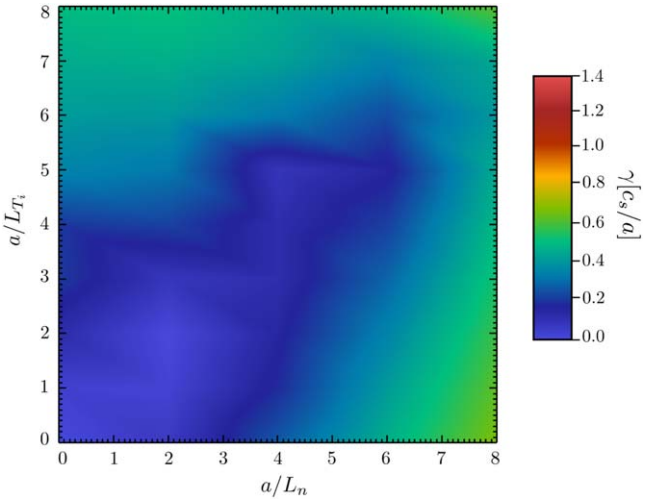

Figure 6. 2D stability map for W7-X high iota configuration including collisions in a Hydrogen plasma, $\nu = 0.057$ in GENE normalized units.

The isotope effect is concentrated in the ion contribution, reducing its magnitude, and in tokamaks, with the TEM usually dominated by the electron contribution, will not produce a strong impact in the linear growth rate. But, in the case of stellarators with a configuration close to maximum-J, like the standard configuration of W7-X, it could be a key factor.

4.3. Effect of collisions

Finally, the inclusion of collisions in the simulations is studied in figure 6. The stability map for the high iota configuration is generated with a collisionality $\nu = 0.057$, a typical value from experiments in GENE units. Comparing the original map with those including collisions, figures 5(a) and 6, we find that collisions tend to considerably reduce the TEM instability, although the valley shape is maintained. In particular, the linear growth rate in the bottom-right corner of the figure 6 is reduced more than 50%, increasing the stability valley conditions along the TEM-dominated region. This is due to the tendency of collisions to de-trap particles, thus reducing the trapped particle population which in turns alleviates the TEM instability [19]. The ITG-TEM mixed modes are also affected, exhibiting a smaller reduction of the linear growth rates in the rest of the stability map, as compared with pure TEM.

5. Conclusions

In this study we have investigated a region of the electrostatic instability space in maximum-J stellarators (in particular for W7-X) which we term 'stability valley', with suppressed micro-instabilities on scales comparable to, or smaller than the ion gyroradius but smaller than the electron gyroradius. The stability valley is present in most configurations of W7-X, and occurs when the normalized temperature and density gradients are similar, i.e. $\eta_i \approx 1$. The width and depth of the valleys vary across configurations, depending on their relative

ability to suppress ITG and TEM instabilities, but in general the valley grows as $\frac{\partial J}{\partial s}$ becomes more negative.

Assuming that the suppression of the micro-instabilities leads to reduced turbulent transport, the properties of the valley could open possibilities for operation with reduced losses, when the appropriate profile conditions are satisfied and sustained in time. From the theoretical perspective, the control of the valley properties is fundamental to extend the region of suppressed micro-instabilities and to facilitate the access to this region. The valley is a mainly geometrical effect, but certain plasma parameters can be used to control its properties, e.g. the normalized ETG can be used to produce the valley at smaller η_i values. The isotope used for the plasma seems to be an important parameter, and heavy isotopes help to produce valley conditions with higher normalized gradients, which we expect to be especially convenient for future W7-X campaigns with Deuterium or reactors powered by Deuterium-Tritium fuel. Finally, it seems that collisions help to reduce TEMs and TEM mixed modes, improving the stability valley conditions in the TEM-dominated region. Preliminary work addressing the role of electromagnetic effects on the structure of the stability valley have shown that, as expected [20], both ITG and TEM instabilities are reduced in large beta conditions. A thorough study of these instabilities, together with the role of kinetic ballooning modes is reserved for an upcoming publication.

Acknowledgments

This work has been carried out within the framework of the EUROfusion Consortium and has received funding from the Euratom research and training programme 2014–2018 and 2019–2020 under grant agreement No 633053. The views and opinions expressed herein do not necessarily reflect those of the European Commission. The GENE simulations have been conducted on the Marconi supercomputer (Italy), and on the Cobra supercomputer (Garching, Germany).

ORCID iDs

J A Alcusón https://orcid.org/0000-0001-5492-7432
P Helander https://orcid.org/0000-0002-0460-590X

References

[1] Hirsch M *et al* 2008 *Plasma Phys. Control. Fusion* **50** 053001
[2] Helander P *et al* 2014 *Rep. Prog. Phys.* **77** 087001
[3] Helander P *et al* 2013 *Phys. Plasmas* **20** 122505
[4] Helander P *et al* 2015 *Nucl. Fusion* **55** 053030
[5] Proll J H E *et al* 2012 *Phys. Rev. Lett.* **108** 245002
[6] Proll J H E *et al* 2016 *Plasma Phys. Control. Fusion* **58** 014006
[7] Plunk G G *et al* 2017 *J. Plasma Phys.* **83** 715830404
[8] Dinklage A *et al* 2018 *Nat. Phys.* **14** 855–60
[9] Beidler C D *et al* 2020 in preparation
[10] Wolf R *et al* 2019 *Phys. Plasmas* **26** 082504
[11] Klinger T *et al* 2019 *Nucl. Fusion* **59** 112004
[12] Geiger B *et al* 2019 *Nucl. Fusion* **59** 046009
[13] Doyle E J *et al* 2007 *Nucl. Fusion* **47** S18
[14] Horton W 2012 *Turbulent Transport in Magnetized Plasmas* (Singapore: World Scientific)
[15] Jenko F *et al* 2000 *Phys. Plasmas* **7** 1904
[16] von Stechow A *et al* 2019 *Density turbulence reduction by equilibrium profile gradient control in 'W7-X' Invited talk, 22nd International Stellarator and Heliotron Workshop 2019 (ISHW 2019) (Madison, WI)* http://hdl.handle.net/21.11116/0000-0004-CF7C-9
[17] von Stechow A *et al* 2020 in preparation
[18] Plunk G G *et al* 2019 *Phys. Rev. Lett.* **122** 035002
[19] Vernay T *et al* 2013 *Plasma Phys. Control. Fusion* **55** 074016
[20] Pueschel M J *et al* 2010 *Phys. Plasmas* **17** 062307